Deep Learning Based Topography Aware Gas Source Localization with Mobile Robot

Changhao Tian[1,2,5,*], Annan Wang[3,*], Han Fan[4,5], Thomas Wiedemann[5,6], Yifei Luo[2], Le Yang[2,7,‡], Weisi Lin[3,‡], Achim J. Lilienthal[4,5,‡], Xiaodong Chen[1,8,‡]

***Abstract*—Gas source localization in complex environments is critical for applications such as environmental monitoring, industrial safety, and disaster response. Traditional methods often struggle with the challenges posed by a lack of environmental topography integration, especially when interactions between wind and obstacles distort gas dispersion patterns. In this paper, we propose a deep learning-based approach, which leverages spatial context and environmental mapping to enhance gas source localization. By integrating Simultaneous Localization and Mapping (SLAM) with a U-Net-based model, our method predicts the likelihood of gas source locations by analyzing gas sensor data, wind flow, and topography of the environment represented by a 2D occupancy map. We demonstrate the efficacy of our approach using a wheeled robot equipped with a photoionization detector, a LIDAR, and an anemometer, in various scenarios with dynamic wind fields and multiple obstacles. The results show that our approach can robustly locate gas sources, even in challenging environments with fluctuating wind directions, outperforming conventional methods by utilizing topography contextual information. This study underscores the importance of topographical context in gas source localization and offers a flexible and robust solution for real-world applications. Data and code are publicly available.**

***Index Terms*—Gas Source Localization, Robot Olfaction, Machine Olfaction, Cognitive Robotics, Deep Learning, Simultaneous Localization and Mapping (SLAM)**

[1]Innovative Center for Flexible Devices (iFLEX), Max Planck-NTU Joint Laboratory for Artificial Senses, School of Materials Science, Nanyang Technological University, Singapore

[2]Institute of Materials Research and Engineering, Agency for Science, Technology and Research, Singapore

[3]College of Computing and Data Science, Nanyang Technological University, Singapore

[4]Robot Navigation and Perception Lab, AASS Research Centre, Örebro University, Sweden

[5]Chair: Perception for Intelligent Systems, MIRMI, Technical University of Munich, Germany

[6]Institute of Communications and Navigation, German Aerospace Center (DLR), Germany

[7]Department of Materials Science and Engineering, National University of Singapore, Singapore

[8]Institute for Digital Molecular Analytics and Science (IDMxS), Nanyang Technological University, Singapore

[*]Changhao Tian and Annan Wang contributed equally to this work.

[‡]Corresponding authors: Le Yang (yang_le@imre.a-star.edu.sg), Weisi Lin (wslin@ntu.edu.sg), Achim J. Lilienthal (achim.j.lilienthal@tum.de), and Xiaodong Chen (chenxd@ntu.edu.sg).

The authors acknowledge the financial support from the Singapore Agency for Science, Technology and Research (A*STAR) under its MTC Programmatic Funding Scheme (project no. M23L8b0049) Scent Digitalization & Computation (SDC) Programme, and the funding from the academic program Sustainable Underground Mining (SUM) project, jointly financed by LKAB and the Swedish Energy Agency.

I. Introduction

In different scenarios, from environmental monitoring [1], industrial safety [2], and disaster rescue [3], dispersed gas is always an important but typically invisible environmental factor. Detecting and locating potential gas sources is crucial for ensuring environmental compliance, preventing industrial accidents, and supporting rescue operations. Therefore, using mobile robots committing gas source localization in hazardous or hard-to-reach environments becomes appealing.

A robot for gas source localization typically uses a gas sensor to detect the gas from the source and an anemometer to estimate the direction of the source. However, real-world scenarios can be challenging as gas source localization is often a non-observable estimation problem [4]. This is because observed gas concentrations and airflow vectors do not directly correlate with the source location due to complex wind-obstacle interactions. Early in gas dispersion, a continuous concentration gradient has not yet formed, and turbulence creates plumes with fluctuating concentrations [5], [6]. This means observed gas concentrations only indicate the presence of gas, not the distance to the source. Additionally, obstacles distort wind streamlines, making it difficult to infer source direction solely from an anemometer. As a result, gas source localization in complex environments with obstacles is challenging due to the limitations of sensory information.

To address this obstacle-induced challenge, we consider leveraging spatial context, such as the environmental topography and observed wind flow, to learn the complex, non-analytical relationship between gas encounters and the actual gas source location. The contextual information in environmental topology can be perceived by Simultaneous Localization and Mapping (SLAM), which allows robots to create or update maps of unknown environments while tracking their location [7]. For gas source localization, SLAM can contribute with accurate locations where gas is detected and corresponding surrounding topography [8]. Assuming that obstacle layout affects the gas dispersal process and, therefore, is crucial for predicting gas source locations, integrating SLAM could greatly enhance the localization process.

In this work, we propose a deep learning-based approach for gas source localization in complex environments. The goal of our work is to train a model that can predict the potential gas source location during the SLAM process when the robot encounters the plume, leveraging data from a LIDAR, an anemometer, and a gas sensor. As depicted in Fig. 1,

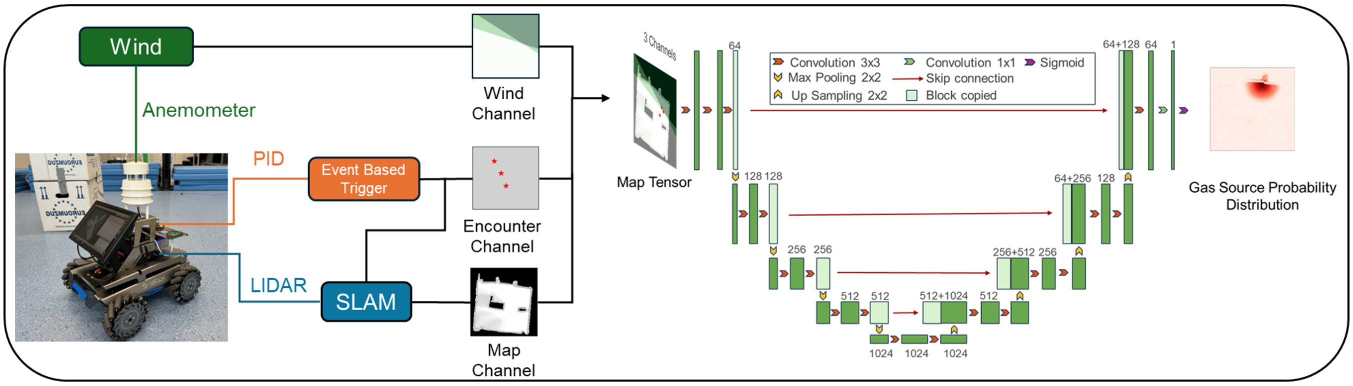

Fig. 1. Overview of the gas source localization system. Our topography-aware approach leverages gas plume encounter data and corresponding contextual information (environmental topography and wind conditions) and can use newly detected gas encounters to predict the gas source location in real-time.

the environment map, gas encounter locations and wind observations will be combined into a 3-channel tensor and put into a U-Net, which can capture the topography context related to gas dispersion. When the robot is deployed to an unknown environment, the model can predict the potential locations of gas sources despite a different topography. To implement and demonstrate our approach, we built a wheeled mobile robot equipped with a photoionization detector (PID), an anemometer, and a LIDAR and conducted real-world experiments. We have shown that our method can locate the gas source effectively in an environment with multiple obstacles and complex gas plume distribution. Even under a changing wind field, our method can remain robust.

The main contribution of this paper is the exploitation of the topography context for gas source localization, which allows our approach to address the challenges posed by the intractable interaction between obstacles and wind fields. This contribution can extend the flexibility and applicability of gas source localization robots in realistic scenarios with the potential of predicting gas source locations from a distance without continuous active tracing.

II. Related Work

The localization of gas sources in complex environments has been a longstanding challenge in the field of mobile robot olfaction. Conventional approaches are unable to handle complex interaction patterns between dispersed gas and environmental topography. Recent advances in deep learning offer a promising solution by approximating these complex patterns and their relationship to the source location, motivating the development of novel learning-based localization approaches.

A. Properties of Gas Plume

In gas source localization, a gas source is typically modelled as a point source with dispersion influenced by flows rather than diffusion. The gas plume can be described as follows: 1) It originates from a point source and follows the wind. 2) Gas concentrations fluctuate due to turbulence, with the highest average concentration along the plume's centerline. 3) Unlike natural diffusion, the plume exhibits patchy concentration levels rather than a smooth gradient. As a result, the presence of a plume is a more reliable indicator of the gas source than the concentration gradient. Some studies model gas plumes analytically [9], [10] or statistically [11], [12], while others focus on plume tracking strategies [6]. Early plume tracking methods aim to keep robots in contact with the plume, such as adjusting speed or direction when losing contact [13], [14]. These methods fall under reactive source localization, discussed in Section II-B.

B. Reactive Gas Source Localization

Reactive methods in robotics involve responding to real-time sensor data with predefined actions, without relying on historical data or dynamic analysis. These approaches are simple, resource-efficient, and adaptable to various platforms [15]. A typical reactive method is chemotaxis [16], where a robot moves toward higher gas concentrations. However, this assumes a continuous concentration gradient, which may not exist in turbulent gas dispersal. An improved version, chemotaxis-anemotaxis [17], uses both gas concentration and wind direction. Bio-inspired strategies like upwind surging and crosswind zigzagging guide the robot [6], [18]. Despite their simplicity, reactive methods often limit flexibility and efficiency, particularly in challenging environments like disaster sites with obstacles and rough terrain. In multi-purpose missions, robots may need to follow specific paths, making it impractical to continuously trace a gas source. In such cases, predicting gas source locations from a distance during exploration becomes more feasible.

C. Statistical Gas Source Localization

Statistical methods address the limitations of reactive approaches by using probabilistic models to estimate the gas source location [4], [19]. These methods integrate sensor data with environmental models and prior knowledge, employing techniques like Bayesian filtering [20], Kalman filtering [21], and particle filtering [19], [22] to update beliefs as new measurements are observed. One state-of-the-art approach, Infotaxis, optimizes source search by maximizing information gain at each step [23]–[25].

In general, statistical methods account for the often meandering and fluctuating gas dispersion and offer the advantage of providing estimates along with uncertainty measures. However, their applicability also has limitations [23], [26].

The major issue is the strong dependence on an accurate gas dispersion model. For example, a common assumption is a uniform wind field, where all points in the field are considered to have the same wind vector. However, this assumption probably will not hold in complex, varying and uncontrolled environmental conditions.

D. Learning-based Gas Source Localization

Deep learning has become a prominent tool in robotic applications due to its ability to make effective decisions with limited data [27]. Methods such as deep Q networks (DQN) [28], [29] and long short-term memory networks (LSTMs) [30] demonstrated promising results in gas source localization problems. Inspired by the success of image segmentation models like U-Net [31], Mask R-CNN [32], and DeepLab [33] in extracting spatial relationships from images, we propose leveraging contextual information embedded in metric maps to enhance gas source localization predictions based on in-situ and sparse observations.

III. Methodology

We develop a gas source localization approach based on an environmental context-aware U-net. The training of the approach is twofold. In the first phase (Section III-A), a series of samples are acquired. Once the robot encounters a gas plume in the environment, the gas sensor signal will be processed by an event-based filter to trigger data collection. Corresponding environmental context, i.e., the current metric map and encounter locations perceived by SLAM, and wind direction from an anemometer will be recorded. In the second phase (Section III-B), we train the U-net to capture the relationship between the environmental context and the source location. The resulting topography-aware U-net is the predictive model that can estimate a probabilistic representation of the gas source location. The model and data for training can be found in https://github.com/CHTiansweet/Topography-aware-Gas-Source-Localization

A. Event-based Human-in-the-loop Data Collection

The model training begins with collecting representative data that encodes the tempo-spatial pattern of plumes released by the gas source. We assume this pattern is indirectly reflected by gas sensor responses, the corresponding position, and observed wind flow when the robot encounters a plume. Plume encounter determination is a two-step process. First, potential encounters are detected using an event-based filter. Then, a human operator validates them to prevent redundant recordings near the same location. The event-based filter, implemented as in Eq. 1 and Eq. 2, follows the approach proposed by Li et al. [34].

$$C_{\text{filtered}} = \begin{cases} 1, & \text{if } c_t > k\bar{c}_{t-1} \\ 0, & \text{if } c_t \leq k\bar{c}_{t-1} \end{cases} \tag{1}$$

$$\bar{c}_t = \gamma\bar{c}_{t-1} + (1-\gamma)c_t \tag{2}$$

where c_t is the sensor response at time t, k is a predefined noise threshold, and γ is a trade-off parameter controlling filter sensitivity. This filter converts continuous sensor readings into binary values indicating plume encounters. With an adaptive threshold $\bar{c}_t$, it detects plumes while mitigating the influence of accumulated gas in the environment. In our experiment, the gas sensor sampling frequency was set to 1Hz, with $\gamma = 0.2$ and $k = 1.04$, determined through preliminary experiments to minimize false positives. When the filter returns 1, the encounter location is recorded after operator confirmation, preventing excessive repeated triggers near the gas source.

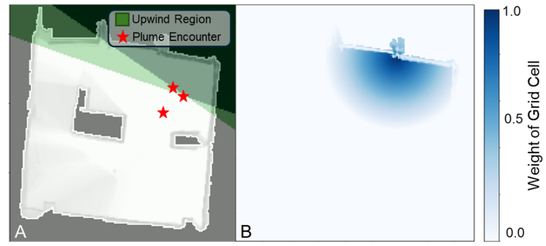

Fig. 2. An example of the map tensor and grid cells' weight in loss calculation. **(A)**: A 3-channel map tensor includes a metric map, gas encounter locations and the wind direction belief. A deeper green colour means a higher belief in the upwind region. **(B)**: An exemplary visualization of the weights of the grids in the loss function. Inside a dynamic detecting range (blue area), grids near the edge will be assigned smaller weights.

Training data collection requires multiple trials. A trial is defined as a mapping process from an initially empty map. When a plume encounter is confirmed, the current occupancy map, the robot's location, and anemometer data are saved. At the trial's end, the robot is guided to the gas source, and its final position on the map is recorded as the true gas source location. Different trials vary in room topography, wind direction, gas source position, and initial robot location.

B. Training Setup

Data Prepossessing: Each recorded gas encounter is stored as a three-channel map tensor: map, gas encounter, and wind. The map channel records the occupancy grid map at the encounter moment, standardized by padding with -1. The robot's position at the gas encounter is defined using the baselink-to-map transformation. The encounter channel, matching the occupancy grid size, marks encounter coordinates with **1**, while other grids remain **0**. All prior encounters are recorded cumulatively. During each trial, samples are sequentially generated in encounter order.

The wind channel plays a key role in gas source localization, assuming gas disperses from upwind to downwind. For a single gas source, the probability of its location in the downwind region relative to an encounter point is lower than in the upwind region. In our wind channel implementation, the anemometer provides a wind vector $\vec{V}_{\text{wind}}$, with wind field matrices matching the map's shape. Each grid cell's value W_i is determined by its orientation relative to the wind: upwind if $\vec{V}_i \cdot \vec{V}_{\text{wind}} \geq 0$, and downwind otherwise. The wind channel accumulates all encountered wind field matrices over time, offering a comprehensive view of wind conditions on the map.

$$W_i = \begin{cases} 1, & \text{if } \vec{V}_{\text{wind}} \cdot \vec{V}_i \geq 0 \\ -1, & \text{if } \vec{V}_{\text{wind}} \cdot \vec{V}_i < 0 \\ 0, & \text{if } \vec{V}_{\text{wind}} = 0 \end{cases} \tag{3}$$

To enhance model robustness, all samples are rotated clockwise by $\frac{\pi}{2}, \pi, \frac{3\pi}{2}$ radians for data augmentation. Fig. 2(A) is a visualization of the map tensor sample corresponding to the 3rd encounter event in a trial.

Source Posterior Map and Loss Function: The model's expected output is a source posterior map, a probabilistic representation of the gas source location. Each grid cell in this map holds a value indicating the probability of containing a gas source, accounting for uncertainty in localization. Since predicting the source location can vary in difficulty depending on encounters and SLAM map completeness, we introduce a dynamic detection range, D_N, defined by Eq. 4, to reduce training instability by adapting based on the number of plume encounters (N) in the current map:

$$D_N = a \cdot e^{-k\cdot(N-1)} + c \tag{4}$$

Here, the parameter a is set to 3, and c is set to 1, meaning that the dynamic detecting range D_N starts at 4 meters after the first encounter and gradually converges to a 1 meter range as the number of encounters increases. k, representing the convergence rate, is set to 0.3. This adaptive range ensures that the model focuses on increasingly smaller and more precise regions as more data is collected, improving localization accuracy over time.

The training loss is defined based on Binary Cross-Entropy (BCE), a commonly used function for binary classification tasks. Instead of focusing on exact source coordinates, our model aims to catch the relevance between the source and the region inside D_N. Standard BCE, given by Eq. 5, is not well-suited for our problem due to the high variability in gas plume encounters and the need to handle spatial uncertainty. To address this, we modify the BCE by introducing a weight that reduces the influence of grid cells near the edges of the detection range, where predictions are less reliable. The proposed modification is critical since manually defined regions are not absolutely accurate, and the model may struggle to align precisely at the edges, leading to instability during training. To ensure smoother training, it is necessary to reduce the weights at the edges of the predicted region.

$$\mathcal{L}_{\text{BCE}}(y_i, \hat{y}_i) = y_i \log(\hat{y}_i) + (1 - y_i)\log(1 - \hat{y}_i) \tag{5}$$

Each grid is assigned a weight according to Eq. 6:

$$y_{N,i} = \begin{cases} 0, & \text{if } d_i > D_N \text{ or } m_i = -1 \\ \frac{(D_N - d_i)}{D_N} \cdot \frac{(100 - m_i)}{100}, & \text{if } d_i \leq D_N \end{cases} \tag{6}$$

in which d_i is the distance between grid i and the gas source location, m_i isthe occupancy probability grid i. Grids outside D_N range of the gas source are labelled as 0, while grids inside D_N range are labelled as $\frac{(D_N - d_i)}{D_N} \cdot \frac{(100 - m_i)}{100}$, considering both distance to gas source and occupancy probability of the map, as shown in Fig. 2(B).

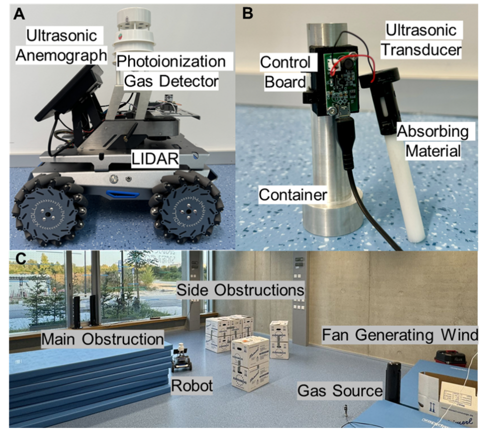

Fig. 3. Experimental setup. **(A)**: The wheeled mobile robot is equipped with a PID, an anemometer, and a LIDAR. **(B)**: The artificial ethanol source. **(C)**: The experiment scenario.

The final training loss is defined by Eq. 7:

$$\mathcal{L} = -\frac{1}{n}\sum_{i=1}^{n} l(y_i, \hat{y}_i) \tag{7}$$

$$l(y_i, \hat{y}_i) = \begin{cases} \mathcal{L}_{\text{BCE}}(y_i, 0), & \text{if } \hat{y}_i = 0 \\ \hat{y}_i^{\frac{1}{5}} \cdot \mathcal{L}_{\text{BCE}}(y_i, 1) \cdot \mathrm{W}_{\text{pos}}, & \text{if } \hat{y}_i > 0 \end{cases} \tag{8}$$

The loss function first computes the binary classification loss for the region in the range D_N, and then adjusts it using the decreased weight $\hat{y}_i^{\frac{1}{5}}$ and a positive weighting factor W_{pos}. $\hat{y}_i^{\frac{1}{5}}$ reduces the weight of predictions near the edges of the detection range, ensuring smoother training and preventing overfitting to noisy data. W_{pos} (set to 5.0) assigns a higher weight to the positive sample in case of imbalanced sample distribution, which ensures that the model pays sufficient attention to the rare but significant positive samples.

Training of Gas Localization Predictive Model: We selected U-Net as our backbone model due to its ability to capture spatial context, handle sparse, irregular data, and perform dense prediction with explainable features. Its encoder-decoder structure with skip connections integrates fine-grained details with global topological features [31]. The dataset was split 4:1 into training and validation sets, ensuring robust evaluation while preventing data leakage by keeping samples from the same trial in the same set. Our U-Net model features a lightweight symmetric encoder-decoder with 23 convolutional layers for deployment on the robot's processor. The encoder has four downsampling steps, each with two 3x3 convolutions, batch normalization, and ReLU activation, with 2x2 max-pooling halving the feature map size at each step. Starting with 64 channels, the count doubles per layer, reaching 1024 at the bottleneck. The decoder mirrors the encoder, using transposed convolutions for upsampling and concatenation with encoder features. A final 1x1 convolution outputs the class probabilities via a sigmoid function. The model converged stably after 100 epochs with a batch size of 8 and an initial learning rate of $1e-5$. Learning rate halving and L2 regularization (weight decay: 0.01) were applied to prevent overfitting.

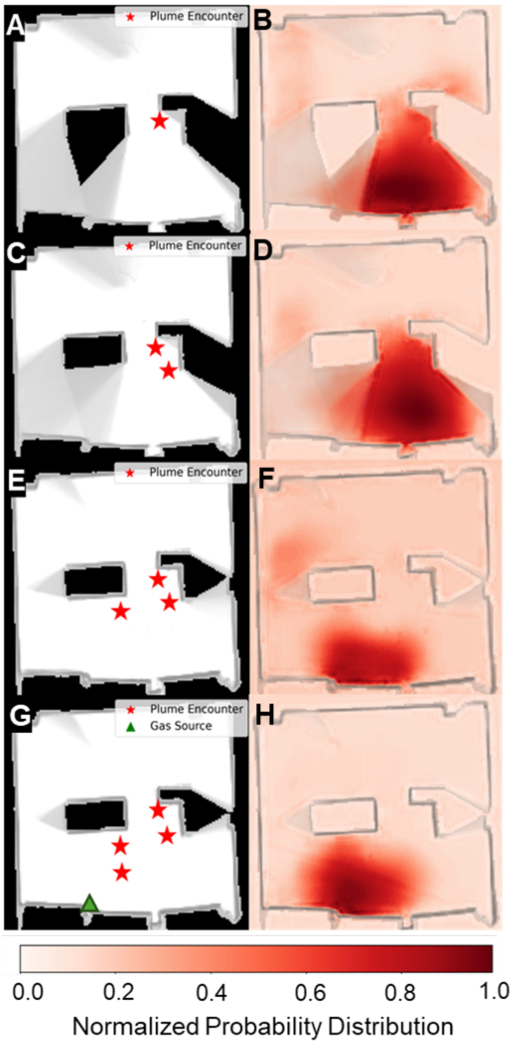

Fig. 4. Model performance in one trial with increasing encounters and map completeness. The model's output demonstrates improved prediction accuracy and continuity as more gas encounters are acquired (Fig. 4(A), (C), (E) and (G)) and the coverage of the source posterior map increases (Fig. 4(B), (D), (F) and (H)). When 4 encounters were acquired (see (Fig. 4(G)), the grids assigned with the highest posteriors in Fig. 4(H) align closely with the actual source.

IV. Experimental Setup

A. Robotic platform and sensor payloads

The robotic platform is built on a Mecanum wheel chassis, shown by Fig. 3(A). It is equipped with a CZ0001 ultrasonic anemometer, an LDS-250D laser LIDAR, and a PID-AH2 gas sensor. The CZ0001 ultrasonic anemometer allows to collect wind in the speed range of 0 to 40 m/s with an angular accuracy of $\pm 2°$, a speed accuracy of $\pm 2\%$ and a speed threshold of 0.05 m/s. The LDS-25D can generate point clouds of up to 14000 points per second with a 30 m range with an accuracy of ± 0.01m at 14k Hz. The PID-AH2 is a highly sensitive photoionization detector (PID). A PID uses an ultraviolet (UV) lamp to ionize a detectable compound, including most Volatile Organic Compounds (VOCs) [35]. In our experiment, the PID-AH2 has a detection range from sub 1 parts per billion (ppb) to 50 parts per million (ppm).

All the sensor payloads are controlled by an NVIDIA Jetson Nano processor. The robot's movement can be controlled via a remote controller. The SLAM functionality was implemented using the Cartographer ROS package [7].

B. Target gas source and area

The target gas is generated by an ultrasonic ethanol vaporizer (see Fig. 3(B)). Ethanol liquid in the container contacts an ultrasonic transducer through an absorbent material, producing ethanol vapour at room temperature. Near the ground surface, the gas can remain at a relatively constant altitude while being dispersed by wind currents without significant vertical floating via temperature gradient.

The experimental setup, depicted in Fig. 3(C), consisted of an empty room measuring 10 meters by 10 meters. To facilitate gas dispersion, an artificial wind field was generated using three fans. A large central obstacle was introduced to alter the overall wind flow pattern, while smaller side obstacles were placed to influence the finer details of the resulting gas plume shape. All obstacles were higher than the fans to prevent airflow from bypassing them. The experiment was conducted under various conditions, including different fan configurations, gas source locations, obstacle arrangements, and initial robot positions

V. Results and Discussion

This section presents the qualitative and quantitative evaluation results of our approach. We conducted 60 trials to gather sufficient training data, and the trained model was then deployed on the robot for gas source localization in real-world trials with previously unseen obstacle layouts and sources. In 8 testing trials with stable wind and 8 testing trials with changing wind, the model successfully inferred gas source locations based on fused map data (see Section V-A). To assess generalization, we tested the model in environments with changing wind fields. As detailed in Section V-B, the results validated the model's robustness, demonstrating its ability to perform fuzzy inference in dynamic environments. The evaluation showcases that spatial context-based inference is an effective approach for gas source localization.

A. Inference with Spatial Context

In testing, our approach performed accurate gas source localization within 4 plume encounters, as the example shown by Fig. 4. This is based on two key factors: a more complete map and an increased number of plume encounter locations. When encountering a plume, the model infers the probability distribution of the gas source within the explored area. Once the environment around the gas source is scanned, from Fig. 4A to Fig. 4C, the distribution becomes more continuous and is associated with a higher confidence level. As the number of encounters increases, the predicted distribution gradually converges, whose high-valued grids begin to overlap on the area surrounding the actual gas source. With a sufficient number of plume encounters, the model gathers enough spatial context to accurately predict the likely gas source area and, therefore potential gas source location.

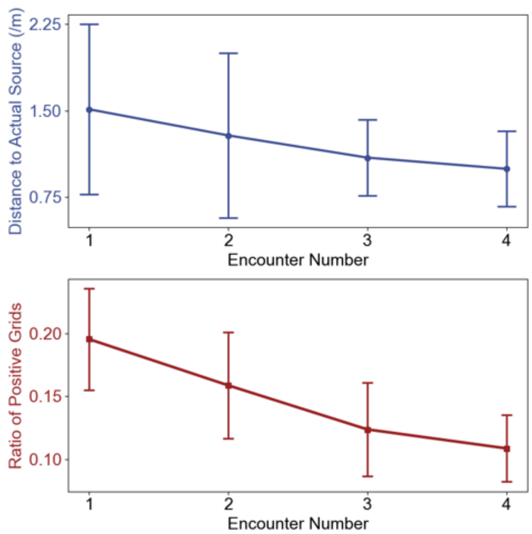

Fig. 5. Quantitative evaluation of the output of the model in testing trials: with increasing number of encounters, both the distance to the actual gas source and the ratio of positive grids decreases, indicating both model's belief and accuracy increase with a more complete spatial context.

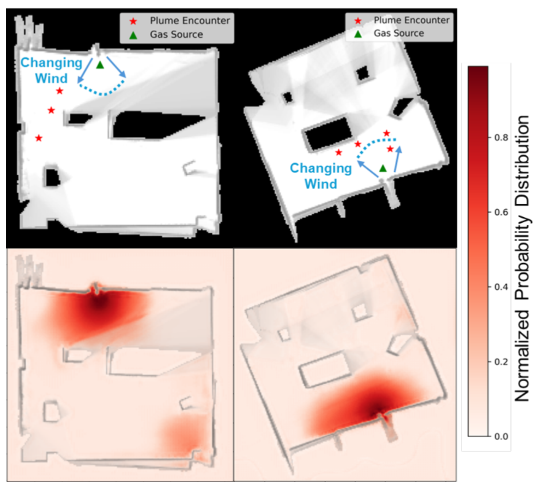

Fig. 6. Results of two test trials posed with changing wind field (shown by blue arrows). In dynamic environments that were never included in the training, our approach remains robust in terms of prediction accuracy.

To evaluate the model's performance, we analyzed how its output evolves with the number of encounters in the testing set. Two indices were defined: the ratio of positive grids and the distance from the probability distribution centroid to the actual gas source. The ratio of positive grids represents the proportion of grid cells with probability values exceeding 0.5, reflecting model confidence. The centroid-based distance quantifies accuracy by weighting each grid cell by its predicted probability. As shown in Fig. 5, after the first encounter, both the mean and spread of the distance to the actual gas source are large, indicating high uncertainty and lower accuracy. As encounters increase, both indices decrease. Notably, the ratio of positive grids drops significantly, showing that the predicted gas source area is converging. Since additional encounters provide more spatial and wind context, this result highlights the importance of contextual information in improving model predictions.

B. Handling Dynamic Wind Fields

To further evaluate the robustness of our method, we conducted tests in dynamic wind fields, where oscillating fans created a swinging wind pattern. As shown in Fig. 6, the robot accurately localized the gas source despite the changing wind conditions in two testing trials. Note that the training data were all generated with non-dynamic wind conditions, and the anemometer can only provide in-situ local airflow measurements. Nevertheless, our approach is still able to perform prediction from encounter events and corresponding contextual information. The success achieved in dynamic wind conditions further emphasizes the importance of spatial context in gas source localization. Our approach is promising with its robustness and broader applicability in complex, uncontrolled real-world environments.

VI. Conclusion and Outlook

In this work, we presented a topography-aware gas source localization approach based on deep learning. Our approach leverages the environmental context to learn the spatial relationship between gas encounter events and the source location. We demonstrated that our method has a robust performance under complex and dynamic conditions in real-world experiments. Our findings suggest that environmental context-based prediction is a promising approach to improving gas source localization of mobile robots.

Currently, the 2D environmental representation relies on the assumption of wind flow around, rather than over obstacles. To achieve more comprehensive gas spatial perception, future work could involve using 3D LIDAR or stereo cameras to obtain a 3D map. Besides, future work will need to address the challenges of multiple or moving gas sources in the environment. Currently, the success of our approach is based on the assumption of a single gas source. When there are multiple potential gas sources of interest, the sufficiency of inferring the gas source location based solely on encounter positions and their contextual information may be challenged.

In future work, we plan to further validate the generalization capability of our approach. Including validation across different distances, scales, and types of environments, such as open spaces, narrow corridors, and areas with irregular obstacles. Additionally, we will conduct a more detailed quantitative evaluation of the model, including ROC curve and ablation experiments. It is worth noting that due to significant differences among various methods—for instance, reactive approaches are evaluated based on the distance between the robot's final position and the gas source [36], there is no standardized benchmark that can be used for a comprehensive comparison across all types of methods. In future work we also plan to design a well-defined gas source declaration procedure to quantitatively assess our approach.

References

[1] T. Lewis and K. Bhaganagar, "A comprehensive review of plume source detection using unmanned vehicles for environmental sensing," *Science of the Total Environment*, vol. 762, p. 144029, 2021.

[2] R. K. Kodali, R. Greeshma, K. P. Nimmanapalli, and Y. K. Y. Borra, "Iot based industrial plant safety gas leakage detection system," in *2018 4th international conference on computing communication and automation (ICCCA)*. IEEE, 2018, pp. 1–5.

[3] H. Fan, V. Hernandez Bennetts, E. Schaffernicht, and A. J. Lilienthal, "Towards gas discrimination and mapping in emergency response scenarios using a mobile robot with an electronic nose," *Sensors*, vol. 19, no. 3, p. 685, 2019.

[4] P. Ojeda, J. Monroy, and J. Gonzalez-Jimenez, "Robotic gas source localization with probabilistic mapping and online dispersion simulation," *IEEE Transactions on Robotics*, 2024.

[5] N. Arnold, J. Gruber, and J. Heitz, "Spherical expansion of the vapor plume into ambient gas: an analytical model," *Applied Physics A*, vol. 69, pp. S87–S93, 1999.

[6] G. Kowadlo and R. A. Russell, "Robot odor localization: a taxonomy and survey," *The International Journal of Robotics Research*, vol. 27, no. 8, pp. 869–894, 2008.

[7] W. Hess, D. Kohler, H. Rapp, and D. Andor, "Real-time loop closure in 2d lidar slam," in *2016 IEEE international conference on robotics and automation (ICRA)*. IEEE, 2016, pp. 1271–1278.

[8] K. Kamarudin, A. Y. Md Shakaff, V. H. Bennetts, S. M. Mamduh, A. Zakaria, R. Visvanathan, A. S. Ali Yeon, and L. M. Kamarudin, "Integrating slam and gas distribution mapping (slam-gdm) for real-time gas source localization," *Advanced Robotics*, vol. 32, no. 17, pp. 903–917, 2018.

[9] H. Ishida, T. Nakamoto, and T. Moriizumi, "Remote sensing and localization of gas/odor source and distribution using mobile sensing system," in *Proceedings of International Solid State Sensors and Actuators Conference (Transducers' 97)*, vol. 1. IEEE, 1997, pp. 559–562.

[10] L. Marques, U. Nunes, and A. T. de Almeida, "Olfaction-based mobile robot navigation," *Thin solid films*, vol. 418, no. 1, pp. 51–58, 2002.

[11] A. J. Lilienthal, M. Reggente, M. Trincavelli, J. L. Blanco, and J. Gonzalez, "A statistical approach to gas distribution modelling with mobile robots-the kernel dm+ v algorithm," in *2009 IEEE/RSJ International Conference on Intelligent Robots and Systems*. IEEE, 2009, pp. 570–576.

[12] M. Reggente, "Statistical gas distribution modelling for mobile robot applications," Ph.D. dissertation, Örebro university, 2014.

[13] H. Ishida, G. Nakayama, T. Nakamoto, and T. Moriizumi, "Controlling a gas/odor plume-tracking robot based on transient responses of gas sensors," *IEEE Sensors Journal*, vol. 5, no. 3, pp. 537–545, 2005.

[14] A. J. Lilienthal, A. Loutfi, and T. Duckett, "Airborne chemical sensing with mobile robots," *Sensors*, vol. 6, no. 11, pp. 1616–1678, 2006.

[15] G. Ferri, E. Caselli, V. Mattoli, A. Mondini, B. Mazzolai, and P. Dario, "A biologically-inspired algorithm implemented on a new highly flexible multi-agent platform for gas source localization," in *The First IEEE/RAS-EMBS International Conference on Biomedical Robotics and Biomechatronics, 2006. BioRob 2006.* IEEE, 2006, pp. 573–578.

[16] W. Jatmiko, K. Sekiyama, and T. Fukuda, "A pso-based mobile robot for odor source localization in dynamic advection-diffusion with obstacles environment: theory, simulation and measurement," *IEEE Computational Intelligence Magazine*, vol. 2, no. 2, pp. 37–51, 2007.

[17] A. Gongora, J. Monroy, and J. Gonzalez-Jimenez, "Gas source localization strategies for teleoperated mobile robots. an experimental analysis," in *2017 European Conference on Mobile Robots (ECMR)*. IEEE, 2017, pp. 1–6.

[18] G. Reddy, V. N. Murthy, and M. Vergassola, "Olfactory sensing and navigation in turbulent environments," *Annual Review of Condensed Matter Physics*, vol. 13, no. 1, pp. 191–213, 2022.

[19] P. P. Neumann, V. Hernandez Bennetts, A. J. Lilienthal, M. Bartholmai, and J. H. Schiller, "Gas source localization with a micro-drone using bio-inspired and particle filter-based algorithms," *Advanced Robotics*, vol. 27, no. 9, pp. 725–738, 2013.

[20] Y. A. Prabowo, R. Ranasinghe, G. Dissanayake, B. Riyanto, and B. Yuliarto, "A bayesian approach for gas source localization in large indoor environments," in *2020 IEEE/RSJ International Conference on Intelligent Robots and Systems (IROS)*. IEEE, 2020, pp. 4432–4437.

[21] J. Ruddick, A. Marjovi, F. Rahbar, and A. Martinoli, "Design and performance evaluation of an infotaxis-based three-dimensional algorithm for odor source localization," in *2018 IEEE/RSJ International Conference on Intelligent Robots and Systems (IROS)*. IEEE, 2018, pp. 1413–1420.

[22] H. Zhu, Y. Wang, C. Du, Q. Zhang, and W. Wang, "A novel odor source localization system based on particle filtering and information entropy," *Robotics and autonomous systems*, vol. 132, p. 103619, 2020.

[23] X.-x. Chen and J. Huang, "Odor source localization algorithms on mobile robots: A review and future outlook," *Robotics and Autonomous Systems*, vol. 112, pp. 123–136, 2019.

[24] T. Jing, Q.-H. Meng, and H. Ishida, "Recent progress and trend of robot odor source localization," *IEEJ Transactions on Electrical and Electronic Engineering*, vol. 16, no. 7, pp. 938–953, 2021.

[25] M. Vergassola, E. Villermaux, and B. I. Shraiman, "'infotaxis' as a strategy for searching without gradients," *Nature*, vol. 445, no. 7126, pp. 406–409, 2007.

[26] T. Wiedemann, "Domain knowledge assisted robotic exploration and source localization," Ph.D. dissertation, Örebro University, 2020.

[27] L. Wang, S. Pang, and J. Li, "Olfactory-based navigation via model-based reinforcement learning and fuzzy inference methods," *IEEE Transactions on Fuzzy Systems*, vol. 29, no. 10, pp. 3014–3027, 2020.

[28] X. Chen, C. Fu, and J. Huang, "A deep q-network for robotic odor/gas source localization: Modeling, measurement and comparative study," *Measurement*, vol. 183, p. 109725, 2021.

[29] T. Wiedemann, C. Vlaicu, J. Josifovski, and A. Viseras, "Robotic information gathering with reinforcement learning assisted by domain knowledge: An application to gas source localization," *IEEE Access*, vol. 9, pp. 13 159–13 172, 2021.

[30] C. Bilgera, A. Yamamoto, M. Sawano, H. Matsukura, and H. Ishida, "Application of convolutional long short-term memory neural networks to signals collected from a sensor network for autonomous gas source localization in outdoor environments," *Sensors*, vol. 18, no. 12, p. 4484, 2018.

[31] O. Ronneberger, P. Fischer, and T. Brox, "U-net: Convolutional networks for biomedical image segmentation," in *Medical image computing and computer-assisted intervention–MICCAI 2015: 18th international conference, Munich, Germany, October 5-9, 2015, proceedings, part III 18*. Springer, 2015, pp. 234–241.

[32] K. He, G. Gkioxari, P. Dollár, and R. Girshick, "Mask r-cnn," in *Proceedings of the IEEE international conference on computer vision*, 2017, pp. 2961–2969.

[33] L.-C. Chen, G. Papandreou, I. Kokkinos, K. Murphy, and A. L. Yuille, "Deeplab: Semantic image segmentation with deep convolutional nets, atrous convolution, and fully connected crfs," *IEEE transactions on pattern analysis and machine intelligence*, vol. 40, no. 4, pp. 834–848, 2017.

[34] J.-G. Li, Q.-H. Meng, Y. Wang, and M. Zeng, "Odor source localization using a mobile robot in outdoor airflow environments with a particle filter algorithm," *Autonomous Robots*, vol. 30, pp. 281–292, 2011.

[35] A. N. Freedman, "The photoionization detector: Theory, performance and application as a low-level monitor of oil vapour," *Journal of Chromatography A*, vol. 190, no. 2, pp. 263–273, 1980.

[36] H. H. Erwich, B. P. Duisterhof, and G. C. de Croon, "Gsl-bench: High fidelity gas source localization benchmarking tool," in *2024 IEEE International Conference on Robotics and Automation (ICRA)*. IEEE, 2024, pp. 17 672–17 678.